HNUE JOURNAL OF SCIENCE DOI: 10.18173/2354-1059.2019-0035
Natural Science, 2019, Volume 64, Issue 6, pp. 93-101
This paper is available online at http://stdb.hnue.edu.vn

A STRUCTURAL CHARACTERIZATION OF MoO_3 MATERIAL PREPARED USING THREE DIFFERENT METHODS

Pham Van Hai and Nguyen Hong Minh Chau
Faculty of Physics, Hanoi National University of Education

Abstract. In this work, we study a semiconductor-based photocatalyst $\mathrm{MoO_3}$ synthesized using three simple techniques, including as-prepared, hydrothermal and microwave-assisted methods. The obtained samples were characterized using X-ray diffraction (XRD), and Raman spectroscopy. We found a better crystallinity in the nanoparticles synthesized by the microwave-assisted method in comparison to those synthesized by the other methods. From this starting result, we chose the microwave-assisted method as a favored one to further investigate the effect of annealed temperatures on the phase formation. In addition, by using the correlation method, we predicted the Raman active modes of α-$\mathrm{MoO_3}$. The results are in good agreement with those obtained by experiments for the same system.
Keywords: Porous $\mathrm{MoO_3}$, microwave-assisted method, hydrothermal method.

1. Introduction

Molybdenum trioxide ($\mathrm{MoO_3}$) is one of the chemical molybdenum compound produced on the large scale due to various applications, including oxidation catalysts, metal-resistant alloys and photocatalysts. $\mathrm{MoO_3}$ crystals are known to exist in three polymorphs, depending on temperature: orthorhombic (α-$\mathrm{MoO_3}$), monoclinic (β-$\mathrm{MoO_3}$) and hexagonal (h-$\mathrm{MoO_3}$) [1-3]. Amongst known phases, α-$\mathrm{MoO_3}$ with an anisotropic layered structure [4] has been widely used as a potential photocatalyst material. Here highly asymmetrical [$\mathrm{MoO_6}$] octahedrons arrange into a bilayer along the (010) direction so that octahedrons with the same corners build up a plane. Compared to the bulk phase, the layered structure $\mathrm{MoO_3}$ gives rise to a significantly larger surface area [5], and consequently is expected to possess a better photocatalytic efficiency.

Until now, a number of experiments have been reported to prepared $\mathrm{MoO_3}$, such as physical vapor deposition (PVD) [6], hydrothermal technique [7], magnetron

Received May 30, 2019. Revised June 20, 2019. Accepted June 27, 2019.
Contact Pham Van Hai, e-mail: haipv@hnue.edu.vn.

sputtering [8], electrocatalytic oxidation [9], chemical precipitation [10] and liquid exfoliation [11]. Yang and coworkers [12] have recently prepared two-dimensional (2D) MoO_3 nanosheets by freeze-drying method, that enables to produce novel porous materials. A great advantage of this technique is that it requires only water as an solvent and use green and sustainable ice crystals. In addition, a variety of pore morphologies and nanostructures of materials can be controlled by simply tuning experimental conditions during freezing. However, to our best knowledge, there is no report in the literature on the preparation MoO_3 materials using the microwave-assisted method, which is an effective route to synthesis the photocatalytic materials [13-17].

In the current work, we prepared porous MoO_3 through a combination of freeze-drying method and thermal annealing. The samples obtained were investigated as a function of experimental conditions and annealed temperatures.

2. Content

2.1. Experiments

**** Materials***

The chemical reagents were analytical grade and were used without further purification.

**** Synthesis of porous MoO_3***

2.5 g Polyvinyl Alcohol (PVA) was dissolved in 50.0 mL of distilled water. Then 5.0 g ammonium molybdate (AHM) was dissolved in 10.0 mL of PVA solution under heating at $80°$C in water bath. When the AHM completely dissolved, the resulting solution was poured into mould and kept for 24h at $0°$C. Differently from a complicated, high-pressure synthesis reported by Yang *et. al.* [12], we skipped the stage at which freeze-drying solution carried out at 80Pa and $0°$C. The freeze-dried samples were divided into three parts that were later used to investigate the effect of experimental setups on the structural property. First part was used without further treatment, called 'as-prepared', the second one was transferred to a 150 mL bottle and heated by a microwave oven at a power of 750 W for 20 min. After microwave processing, the solution was naturally cooled down to room temperature. The third part was inserted into a thermo flask to used for hydrothermal synthesis at $160°$C for 8 hours [18]. Finally, all the powers obtained from three parts were annealed for 5 h at different temperatures from $300°$C to $600°$C with a heating rate of $10°$C/min^{-1} in air.

**** Characterization***

The obtained samples were characterized by powder X-ray diffraction (XRD) on a Siemens D5005 X-ray diffractometer. The Raman spectroscopy analysis was performed with a Horiba LabRAM HR Evolution spectrometer at an excitation wavelength of 532 nm.

2.2. Results and discussion

2.2.1. Prediction to Raman active modes

There are many different approaches to predict the Raman active modes: a purely mathematical one, using the correlation method, a classical one based on GF Wilson's method and a quantum one based on the ab initio calculations. The first one is accurate because it is purely symmetric but does not allow to determine the vibrational frequency and intensity of Raman modes. The second one uses the extended to crystals GF Wilson's method, but it's emprical. The third one has several approximations (Born–Openheimer, correlation, basis for quantum states). A large number of programs calculates the vibrational frequencies from the first principles by using DFT which is quite reliable, such as DMol, Quantum Expresso, Siesta, VASP.

Here, for sake of simplicity, based on the group theory and Halfords site symmetry correlation method, we calculate the Raman active modes of $\mathrm{MoO_3}$. The details are given as follows:

First, it is known that the number of molecules in crystallographic unit cell (Z) and the number of lattice points (LP) of the $\mathrm{MoO_3}$ crystal are 4 and 1, respectively. Therefore, the number of molecules in the Bravais space cell is $Z_B = \dfrac{Z}{LP} = 4$. The equilibrium position of each atoms lies on a site that has its own symmetry. This site symmetry, a subgroup of the full symmetry of the Bravais unit cell, must be ascertained correctly for each atom. The space group of the $\mathrm{MoO_3}$ is Pnma D_{2h}^{16} with site symmetries $2C_i(4)$; $C_s(4)$; $C_1(6)$. Note that $C_i(4)$ indicates that there are four equivalent atoms occupying sites of symmetry C_i. The coefficient 2 shows the presence of two different and distinct kinds of C_1 site in this unit cell. Each can accommodate four equivalent atoms.

Using the correlation methods with a data combination of Tables 1-4, we predict active IR and Raman modes, given as follows:

$$\Gamma = 8A_g + 8B_{1g} + 4B_{2g} + 4B_{3g} + 4A_u + 3B_{1u} + 7B_{2u} + 7B_{3u} \tag{2.1}$$

where A_g; B_{1g}; B_{2g}; B_{3g} represents Raman-active modes, A_u is an inactive mode for both Raman and IR, B_{1u}; B_{2u}; B_{3u} are infrared-active modes. Therefore, there are 24 Raman active modes for orthogonal crystals $\mathrm{MoO_3}$.

Table 1. Wyckoff site for atoms in MoO_3

Symmetric position	No.	Wyckoff site	Atoms
$2C_i(4)$	$C_i(4)$	a	
	$C_i(4)$	b	
$C_s(4)$	$C_s(4)$	c	Mo;O
$C_1(6)$	$C_1(6)$	d	

Table 2. Symmetric group of MoO_3

Atoms	**Symmetric position**		**Translation**	$\mathbf{t}^{\xi}$	$\mathbf{f}^{\xi} = \mathbf{nt}^{\xi}$
Mo	C_s	A'	T_x, T_y	2	8
		A''	T_z	1	4
O	C_s	A'	T_x, T_y	2	24
		A''	T_z	1	12

Table 3. The correlations of atom Mo in MoO_3 material

f^{ξ}	t^{ξ}	C_i	D_{2h}	C^{ξ}	a^{ξ}
8	2	A'	A_g	1	2
			B_{1g}	1	2
			B_{2u}	1	2
			B_{3u}	1	2
4	1	A''	B_{2g}	1	1
			B_{3g}	1	1
			A_u	1	1
			B_{1u}	1	1

Table 4. The correlations of atom O in MoO_3 material

f^{ξ}	t^{ξ}	C_i	D_{2h}	C^{ξ}	a^{ξ}	$a_{A'}$	$a_{A''}$
24	2	A'	A_g	1	6	6	0
			B_{1g}	1	6	6	0
			B_{2u}	1	6	6	0
			B_{3u}	1	6	6	0
12	1	A''	B_{2g}	1	3	0	3
			B_{3g}	1	3	0	3
			A_u	1	3	0	3
			B_{1u}	1	3	0	3

2.2.2. Experimental results

**** Raman spectrum for MoO_3***

To compare with the theoretical calculation, we choose a $\mathrm{MoO_3}$ sample synthesized by the microwave-assisted method at $400°$C as a reference sample. Figure 1 shows the Raman spectrum of the $\mathrm{MoO_3}$ in the range from 80-1100 cm^{-1}. The spectrum shows the peaks in mult- bands at around 82 cm^{-1}, 97 cm^{-1}, 116 cm^{-1}, 128 cm^{-1}, 157 cm^{-1}, 197 cm^{-1}, 217 cm^{-1}, 244 cm^{-1}, 286 cm^{-1}, 336 cm^{-1}, 365 cm^{-1}, 378 cm^{-1}, 471 cm^{-1}, 665 cm^{-1}, 817 cm^{-1} and 994 cm^{-1}, in good agreement with the characteristic peaks of α-orthogonal $\mathrm{MoO_3}$ [16, 17]. Specifically, in the bands 600-1000 cm^{-1}, the strongest

intensity peak is located at around 817 cm^{-1}, attributed to the stretching vibration of Mo–O bonds (A_g mode) along the b axis of the $\mathrm{MoO_3}$ orthorhombic crystal structure and symmetrical elasticity of oxygen atoms (B_{1g} mode). The peak at 994 cm^{-1} position (A_g, B_{1g}) corresponds to the asymmetric oscillation of the atomic oxygen atomic terminal, which can be recognized as the stretching vibration of Mo–O bonds (A_g) along the a axis of the $\mathrm{MoO_3}$ orthorhombic crystal structure. The peak 665cm^{-1} (B_{2g}, B_{3g}) is the asymmetric elastic stretching modes of the demand Mo–O–Mo along the c-axis. In the range of 400 - 600 cm^{-1}, the peak 471 cm^{-1}(A_g) presents O–M–O stretching and bending. At wavenumbers below 200 cm^{-1}, the peaks around 116 cm^{-1}, 128 cm^{-1} and 157 cm^{-1} originate from the translational (T_c) rigid $\mathrm{MoO_4}$ chain mode (B_{2g}), the translational (T_c) rigid $\mathrm{MoO_4}$ chain mode (B_{3g}) and the translational (T_b) rigid $\mathrm{MoO_4}$ chain mode (A_g, B_{1g}). The Raman peaks 197 cm^{-1}(B2g) contribute from O=Mo=O twisting modes. The peaks at 378 cm^{-1} (B_{1g}) and 365cm^{-1} (A_g) correspond to the O2=Mo=O2 scissor oscillation, the peak at 336 cm^{-1} (A_g, B_{1g}) belongs to the O3MO3 bending. The peak at 286 cm^{-1} is the oscillation of the double bond O=Mo= O corresponding to the O1=Mo=O1 wagging B_{2g} and B_{3g}, respectively. The peaks at 244, 217 cm^{-1} correspond to the B_{3g}, A_g modes, respectively, due to the O2–Mo–O2 scissor.

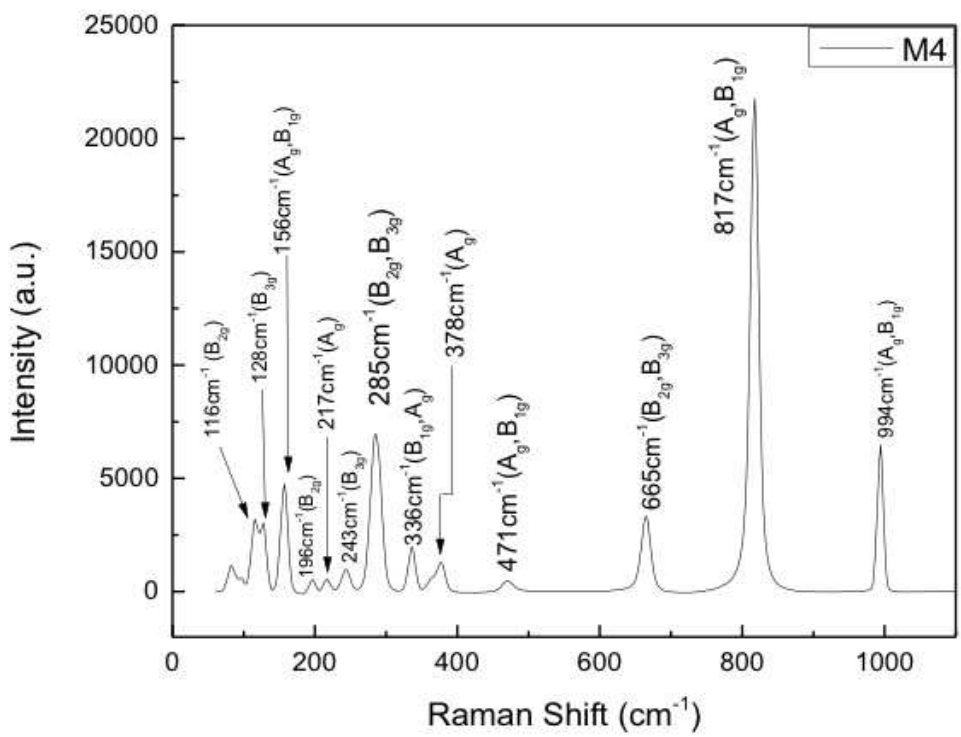

Figure 1. The Raman spectrum of MoO_3 and its mode assignment

Compared to a number of 24 possible Raman-active modes from the theoretical calculation, we observed 20 Raman modes from our experimental data. This may result

from the fact that the remaining four modes have so low intensity that they cannot be detected in the experimental setups. It should be noted that the Raman intensity is affected by various factors. Given a certain condition of the laser wavelength, power and sample concentration, the intensity of the Raman peak is still a complicated function of many parameters [19],

$$I_k = \frac{N(v_k - v_0)^4 S_k Q_k^2 P}{\left[1 - \exp\left(\frac{-hcv_k}{kT}\right)\right]}$$

where N is a proportionality constant, v_0 is the exciting laser wavenumber, v_k is the wavenumber of the vibrational mode, c is the speed of light, h and k are Plancks and Boltzmanns constants, T is the temperature, P is the exciting laser irradiance, and Q_k^2 is an amplitude factor. In principle, in order to detect the weak Raman intensity, we can employ a higher laser power, increase the integration time or use different exciting wavelengths to suppress the photolumninescence bands of the sample.

**** The effect of preparation conditions on the structural characterization***

Figure 2a shows Raman scattering spectra of $\mathrm{MoO_3}$ at different experimental conditions, including the sample using the as-prepared, hydrothermal and microwave methods prepared at $400°$C. As can be seen, all of three samples exhibit the characteristic peaks of α-$\mathrm{MoO_3}$, indicating that the nano-crystal $\mathrm{MoO_3}$ nano-materials have successfully synthesized. However, at the same experimental conditions, the intensity and FWHM of various peaks (at around 82cm^{-1}, 217cm^{-1} and 471cm^{-1}) in the samples prepared by the hydrothermal method is relatively low compared to those in the samples prepared by the as-prepared and microwave-assisted method. This result suggests that the crystalline quality of $\mathrm{MoO_3}$ is improved in the two latter cases. In addition, our result also indicates the microwave-assisted method provides the highest crystalline quality. Figure 2b shows XRD of $\mathrm{MoO_3}$ samples corresponding to three methods as mentioned above. It can be observed that all the $\mathrm{MoO_3}$ samples have the characteristic peaks at $12.7°$; $23.4°$; $25.7°$; $27.4°$; $29.8°$; $33.7°$; $35.5°$ corresponding to the Miller plane, such as (020), (110), (040), (021), (130), (111), (041), indicating a high crystallize quality and a relatively large nanoparticle sizes of $\mathrm{MoO_3}$ [20].

We determine the approximate particle size of $\mathrm{MoO_3}$ from X-ray diffraction diagram based on the full width the half maximum (FWMH) according to the Scherrer formula with $D = \dfrac{0.89\lambda}{\beta\cos\theta}$, where λ (1.54 Å) is the X-ray wavelength, β is the line broadening at FWHM, and θ is the Bragg angle. In Table 5, we show the average particle sizes for three different methods. Apparently, the hydrothermal method produces the largest particles size, in contrast to the particle sizes prepared using the microwave-assisted method. Our results show a good agreement with those obtained from the analysis of Raman spectra.

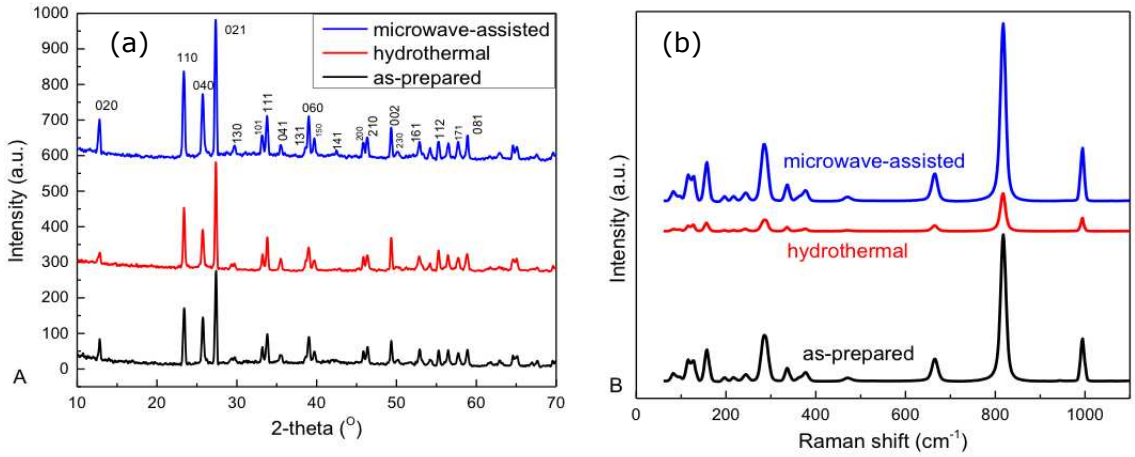

Figure 2. a) XRD pattern and (b) Raman spectrum of MoO_3 synthesized by three methods: as-prepared, hydrothermal and microwave methods.

Table 5. The average particle size of MoO_3 prepared using different methods

Prepared by	2θ	(hkl)	β (in°)	β (rad)	D (nm)
As-prepared	23.4	110	0.29	0.0051	29
Hydrothermal	23.4	110	0.25	0.0043	34
Microwave	23.45	110	0.47	0.0082	18

**** The effect of annealed temperature on the structural characterization***

Because of the best crystallinity for the sample synthesized by the microwave-assisted method, we choose it to further investigate the influence of annealed temperatures on the structural properties of MoO_3.

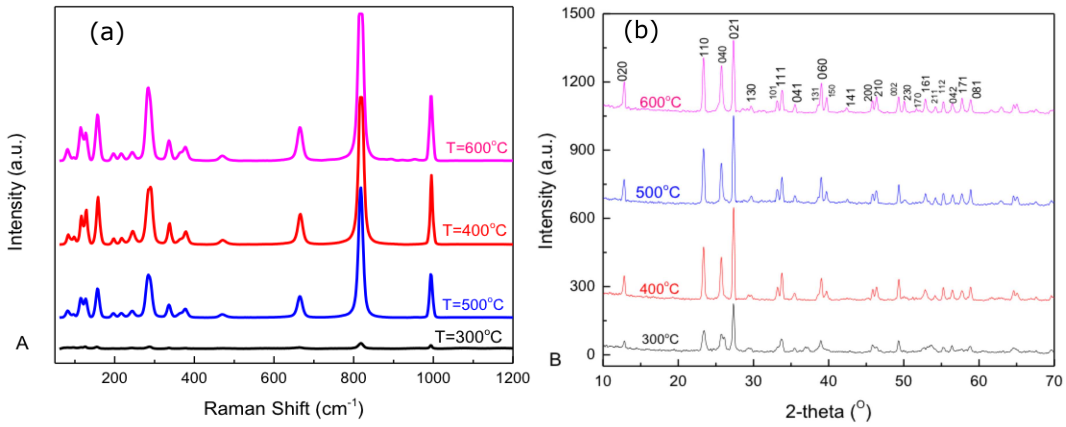

***Figure 3. a) Raman spectrum and b) XRD pattern of MoO_3 synthesized by the microwave method and calcined at several temperatures* 300°C, 400°C, 500°C, 600°C**

Figure 3 displays the Raman spectra and XRD for nanocrystal MoO_3 annealed at several distinct temperatures from 300 to $600°$C. We observe peak intensities in the both Raman and XRD data even at $300°$C calcined temperature, that can be well indexed to the α-orthorhombic structure with the lattice parameters and the unit cell volume were found to be a = 4.00 Å, b = 13.967 Å, c = 3.710 Å. However, the Raman and XRD peaks in the sample calcined at $300°$C are not clearly distinct as those in the sample calcined from $400°$C to above. A further increase in the annealed temperatures allows the crystallite to nucleate, develop along precise growth sites, and assemble orderly, thus, promoting high crystalline samples.

3. Conclusion

In this work, we have conducted research on produced MoO_3 based on few distinct approaches, including as-prepared, hydrothermal and microwave methods. We also investigate the role of calcinated temperature on the phase formation of MoO_3. Here is some conclusions draw: (i) the MoO_3 materials have been successfully synthesized using three simple strategies. All samples obtained show a good crystalline quality and nanoparticles in the range 20-40 nm. (ii) The theoretical calculation according to the group theory gives rise to 24 Raman active modes, in agreement with a majority number of Raman modes obtained from the experimental results. Four missing modes in the experimental data are A_g and B_{1g}. (iii) At the same measurement parameters of Raman and XRD, we find a better crystallinity in the sample prepared by the microwave-assisted methods compared to those obtained from as-prepared and hydrothermal methods. (iv) An investigation on the temperature dependence of the phase formation shows that the MoO_3 has a α-orthorhombic. At higher temperatures, there is an improvement of crystallinity degree.

REFERENCES

[1] Gaigneaux, E. M., Fukui, K. and Twasawa, Y., 2000. Thin Solid Films., **374**, 49.
[2] Lin, S. Y. *et al*., 2010. J. Sol-Gel Sci. Technol., **53**, 51.
[3] Manivel, A. *et al*., 2015. Mater. Res. Bull., **62**, 184.
[4] Xia, Y. C., Wu, C. S., Zhao, N. and Zhang, Y. H. Spongy, 2016. Mater. Lett., **171**, 117.
[5] Cheng, L., Shao, M. W., Wang, X. H. and Hu, H. B, 2009. Chem. Eur. J., **15**, 2310.
[6] Sharma, R. K. and Reddy, G. B., 2014. J. Alloy. Compound., **598**, 177.
[7] Schuh, K. *et al.*, 2015. J. Solid State Chem., **119**, 11792.
[8] Ma, Y., Zhang, X., Yang, M. and Qi, Y. X., 2014. Mater. Lett., **136**, 146.
[9] Zhang, H. L. *et al.*, 2015. Appl. Surf. Sci., **356**, 294.
[10] Chithambararaj, A., Sanjini, N. S., Velmathi, S. and Chandra, B. A., 2013. Phys. Chem. Chem. Phys., **15**, 14761.

[11] Zhang, H. J., Gao, L. J. and Gong, Y. J., 2018. Electrochem. Commun., **52**, 67.
[12] Yang Liu, Peizhong Feng, Zhang Wang, Xinyang Jiao and Farid Akhtar, 2017. Scientific Reports, **7**, 1845.
[13] Luc Huy Hoang *et al.*, 2018. Materials Chemistry and Physics, **221**, 197.
[14] Luc Huy Hoang, Nguyen Dang Phu, Heng Peng, Xiang-Bai Chen, 2016. Journal of Alloys and Compounds, **744**, 228.
[15] Luc Huy Hoang *et al*., 2016. Journal of Materials Science: Materials in Electronics, **27**, 6452.
[16] Lupan, V Trofim, V Cretu, I Stamov, N N Syrbu, I Tiginyanu, Y K Mishra and R Adelung., 2014. Journal of Physics D: Applied Physics, **47**, 085302.
[17] Liu *et al.*, 2009. Journal of Applied Physics, **105**, 023513.
[18] Luc Huy Hoang *et al.*, 2019. HNUE Journal of Science, **64**, 45.
[19] Elena E. Zvereva, Artur R. Shagidullin, and Sergey A. Katsyuba, 2011. Journal of Physical Chemistry A, **115**, 63.
[20] Mauro Epifani, Patrizia Imperatori, Luciana Mirenghi, Monica Schioppa, Pietro Siciliano, 2004. Chemistry of Materials, **16**, 5495.